Mode-converted Lamb wave sensitivity prediction for part-thickness crack-like defects

L. Lijian, P. Fromme

L. Lijian, P. Fromme, "Mode-converted Lamb wave sensitivity prediction for part-thickness crack-like defects," Proc. SPIE 12488, Health Monitoring of Structural and Biological Systems XVII, 1248821 (25 April 2023); doi: 10.1117/12.2657951

Event: SPIE Smart Structures + Nondestructive Evaluation, 2023, Long Beach, California, United States

Mode-converted Lamb wave sensitivity prediction for part-thickness crack-like defects

L. Lijian and P. Fromme
Department of Mechanical Engineering, University College London, WC1E 7JE, UK

ABSTRACT

Fatigue crack growth is one of the most common damage types in aluminum components, widely used in aircraft structures. Detection of fatigue cracks at an early stage is important to guarantee aircraft safety. Efficient non-destructive evaluation (NDE) and structural health monitoring (SHM) can be achieved by employing low frequency guided ultrasonic waves, as they can propagate long distances along plate structures. SHM systems using distributed guided waves sensors have been proposed for efficient monitoring, but have limitations due to environmental influences such as the temperature stability of the conventional baseline subtraction method. The scattering and mode conversion of guided waves at part-thickness defects was investigated to quantify the sensitivity for defect detection and the potential for the development of a baseline-free SHM methodology employing mode converted guided waves. Baseline-free SHM methodology employing mode conversion is expected to overcome some of the limitations caused by environmental factors and to improve sensitivity and stability by employing new or modified signal processing algorithms. A three dimensional (3D) Finite Element (FE) model was developed to predict the mode conversion of the fundamental guided wave modes. The influence of defect length and depth on detection results were investigated numerically. The detection sensitivity for part-thickness defects in a plate is quantified.

Keywords: Mode conversion, Lamb waves, Finite element analysis, Structural health monitoring

1. INTRODUCTION

Fatigue cracks are a very common problem in aerospace operation and maintenance, as fatigue causes 60% of the total service failures in aircraft components [1]. Fatigue, the weakening of the material, occurs under external cyclic loading [2] and fatigue cracks initiate at a microscopic level [3]. Non-destructive evaluation (NDE) identifies and characterizes the damage without harming the specimen [4].

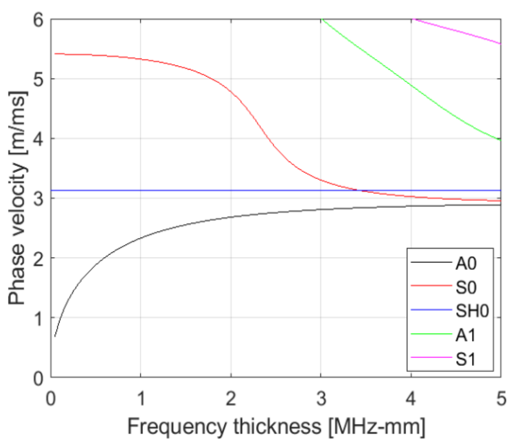

(a)

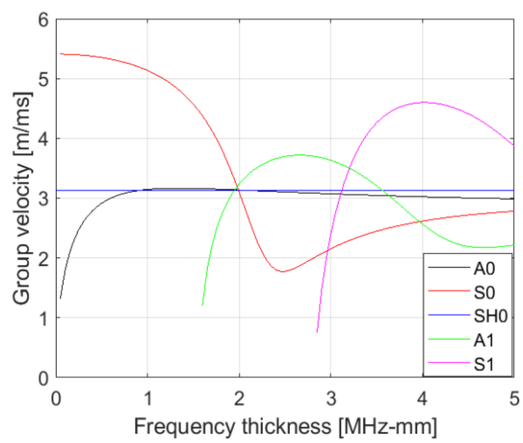

(b)

Figure 1. Dispersion diagram for aluminum plate: (a) phase velocity; (b) group velocity.

Health Monitoring of Structural and Biological Systems XVII, edited by
Paul Fromme, Zhongqing Su, Proc. of SPIE Vol. 12488, 1248821
© 2023 SPIE · 0277-786X · doi: 10.1117/12.2657951

Guided waves can provide rapid and cost-efficient structural health monitoring (SHM), as they can propagate significant distances along large, thin structures with little attenuation [5]. Lamb waves are elastic waves that propagate in isotropic plate structures [6]. There are two types of Lamb wave modes, symmetric and anti-symmetric. At low frequencies, below the cut-off frequencies of higher wave modes, the fundamental symmetric (S_0) mode has the advantage of having the fastest and similar phase and group velocity, and not being very dispersive, as shown in Fig. 1. It is the first arrival wave mode and thus can be distinguished easily [7]. Compared with the S_0 mode, the fundamental anti-symmetric (A_0) mode was found to be more sensitive to small size defects because of the smaller wavelength at the same frequency. However, it has the disadvantage that it is dispersive, i.e., the wave shape keeps changing as it propagates along the plate. The group velocity of the A_0 mode above 0.5 MHz-mm frequency thickness product is reasonably constant and not too much pulse distortion occurs [8]. Compared with Lamb waves, the fundamental shear horizontal wave mode (SH_0) is non-dispersive, which makes the signal analysis easier as the pulse shape does not change. The particle vibrations of the SH_0 mode are perpendicular to the propagation direction. At low frequencies, the main displacement of the S_0 and SH_0 modes is in-plane, while for the A_0 wave mode the out-of-plane displacement is dominant (Fig. 2).

Guided wave scattering patterns at defects and the influence of different parameters on detection results were studied. The perpendicular reflection and transmission of the S_0 [9], A_0 [10], and SH_0 [11] modes at part-thickness notches in a steel plate were investigated. For the S_0 mode, the sensitivity increased as the frequency-thickness product increased. For the A_0 mode, the sensitivity increased as the frequency increased, but decreased once beyond the cut-off frequency of higher wave modes. A deep crack (e.g., 75% of thickness) had a higher detection sensitivity than a shallow crack (31% of thickness) for both wave modes. For the SH_0 mode, the sensitivity was almost constant as the frequency-thickness increased. The interaction of the S_0 mode with through-thickness cracks of different sizes was investigated [12]. The sensitivity increased with the increase in defect length as expected in general and was frequency independent. The guided wave scattering at crack-like defects in an aluminum plate structure was studied [13]. The influence of defect length, defect depth, and incident wave angle on the A_0 wave mode detection results were investigated. Good agreement between Finite Element (FE) simulation and experimental results was obtained. For a perpendicular incident wave and shallow defects, the maximum scattered amplitude was observed in the forward direction. The maximum amplitude increased linearly as the defect depth increased. The maximum amplitude of the scattered wave continued to increase with defect length, but with steps rather than linearly. The scattering of the SH_0 wave mode at a through-thickness [14, 15] and part-thickness [16] notch in an aluminum plate structure was studied. When the monitoring distance was larger than $l^2/4\lambda$ (defect length l, wavelength λ), the sensitivity linearly increased as the defect length increased or as the center frequency increased for through-thickness notches. For part-thickness notches, a deeper defect gave a higher sensitivity. With the defect length increasing, the sensitivity initially increased linearly and then decreased.

When guided waves propagate along a plate and encounter part-thickness defects, part of the energy can be transferred to other guided wave modes. This phenomenon is called mode conversion [17]. Guided wave mode conversion (S_0 mode to A_0 mode) at part-thickness holes [18] and crack-like defect localization [19] in a plate were studied. The defect location could be successfully detected by the time reversal of the mode converted scattered Lamb waves (A_0 mode). A baseline-free mode converted (S_0 mode to A_0 mode) part-thickness crack detection technique was experimentally validated [20].

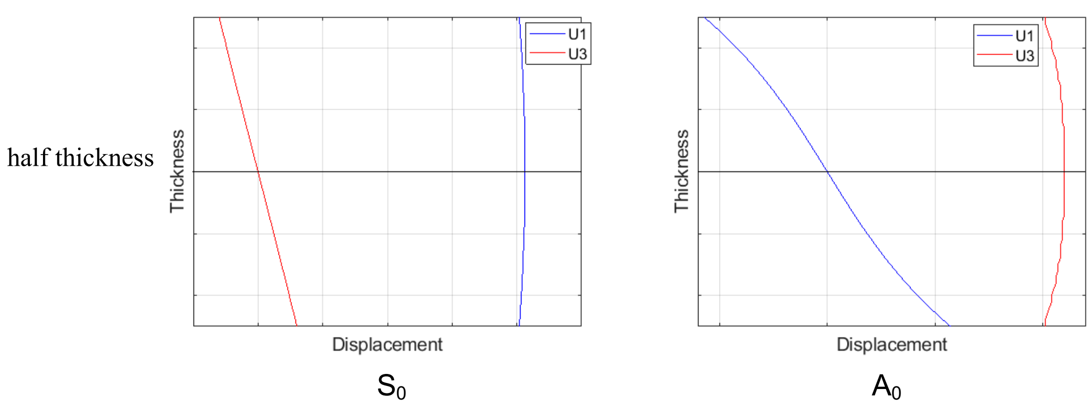

Figure 2. Mode shape structure for fundamental Lamb wave modes at 0.5MHz-mm in aluminum plate; red line: out-of-plane displacement (U_3); blue line: in-plane displacement (U_1).

The fundamental guided wave modes have been widely studied and used for the detection of defects in a plate, but the mode conversion of guided waves has not been widely investigated for plate structures. For mode conversion, the influence of different parameters of defect and excitation settings on the detection results and scattering patterns should be investigated. In this work, the FE simulations and signal processing to numerically investigate guided wave scattering and mode conversion were described in section 2. The analysis for mode conversion from the A_0 mode to the S_0 and SH_0 modes with a focus on separation of the latter two modes was provided in section 3. In section 4, the influence of the defect depth and length on detection results (A_0 to S_0 mode) was investigated.

2. FINITE ELEMENT SIMULATIONS

The aim of the FE simulation was to model the guided wave scattering, understand the mode conversion and scattering patterns, and to investigate the influence of crack and incident wave parameters on detection sensitivity. MATLAB was used to generate the input files for FE simulations in ABAQUS/Explicit. This allows for the model parameters to be conveniently and effectively controlled, as it is not necessary to define a new geometry in ABAQUS/CAE for changes of the defect geometry. Uniform node numbering is used with MATLAB, allowing full control for accurate and repeatable placement of nodal output requests. The standard plate size was chosen as 1500mm x 1000mm x 5mm, large enough to avoid overlap in the time domain with reflections at the plate edge. 8-node linear brick elements with reduced integration (C3D8R, $\triangle x=\triangle y$=1mm, $\triangle z$=0.625mm) were used because the element size should be less than 1/10th of the shortest wavelength (A_0 wave mode: 19mm at 100kHz) to obtain accurate FE results [13]. An even number of elements through the plate thickness is advantageous for the representation of the through-thickness mode shapes (symmetric or anti-symmetric) and eight elements ($\triangle z$=0.625mm) through the plate thickness (5mm) were sufficient to model and investigate the part-thickness defect. Material properties of aluminum (density: 2800kg/m^3, Young's modulus: 73GPa, Poisson's ratio: 0.33) were used to define the modeled isotropic, elastic plate. No damping was assumed with zero Rayleigh damping ($\beta = 0$).

The scattering and mode conversion from an excited A_0 wave mode pulse to the S_0 and SH wave modes was simulated and evaluated. An out-of-plane point force excitation was applied at a node 300mm from the defect location to obtain limited curvature of the (ideally plane) incident wave front. The number of cycles of the narrowband excitation pulse (sinusoid in a Hanning window) was set at five and the center frequency was 100kHz. This gives a frequency thickness product of 0.5MHz-mm, with limited distortion of the A_0 and S_0 wave modes (Fig. 1). The amplitude of the excitation signal, *x(t)* is given by

$$x(t) = 0.5\,(1 - cos\,(\frac{2\pi f t}{N}))sin\,(2\pi f t) \qquad (1)$$

where f is the center frequency, t is time, and N is the number of the cycles.

The defect was located at the x=900mm, y=500mm position (from corner of plate) and the point excitation location was applied at x=600mm, y=500mm. The defect size was varied in length (6 to 50mm) and depth (0 to 5mm). The defect was modeled as a notch by removing one row of the brick elements. The notch width was set to 1mm with right-angle corners. A notch instead of a fatigue crack (zero width) was investigated, as it is easier to create for the experimental validation. As the notch width is significantly smaller than the wavelength, no significant difference is expected, but this will need to be verified at a later stage. Mesh refinement around the defect was not implemented as a regular Cartesian mesh was previously found to be sufficient [13]. Explicit time integration with a time step of 0.1µs was used and the total simulation time period was 0.3ms. The time step is small enough that the wave has not propagated across a complete element within one time step to avoid stability problems [13]. The stability criteria for the FE simulation have been fulfilled for element size and time step. Free boundary conditions were applied to the plate.

A monitoring circle with 300mm radius around the defect was used to collect data with monitoring points every 5° (totally 72 points). The time domain history output data displacements for each monitoring point were extracted from ABAQUS as a report file. The report file was read and the data saved in MATLAB format for analysis. For the displacement data, the Fast Fourier Transform (FFT) was used to obtain the complex magnitude (amplitude and phase angle) for each monitoring point at the center frequency.

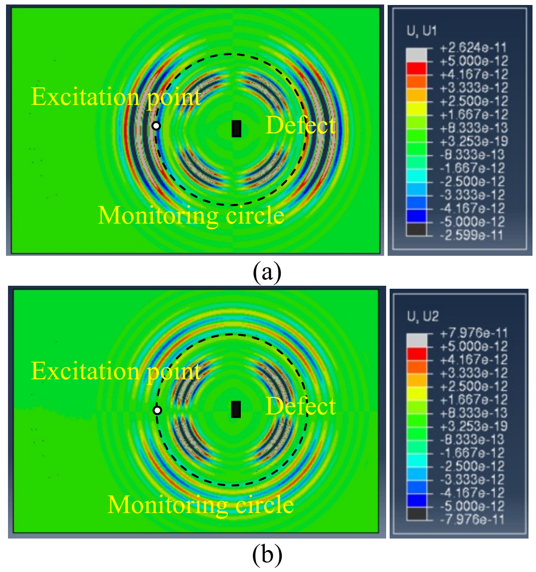

Figure 3. Half-thickness cut-view time snapshots (at 0.2ms) of FE damaged plate simulation showing displacement with out-of-plane point force: (a) U_1 component; (b) U_2 component; excitation location, defect, and monitoring circle indicated.

3. MODE CONVERSION FROM THE A_0 TO S_0 AND SH_0 MODE

Figure 3 shows time snapshots (0.2ms) for a perpendicular incident A_0 wave mode from the 0° (horizontal) direction on a 20mm long vertical defect with a depth of 2.5mm (half plate thickness). The figure panels show the respective in-plane (U_1, U_2) displacements at the half thickness of the plate, where respectively the A_0 and S_0 modes have only an out-of-plane or in-plane component (see Fig. 2). The mode converted scattered S_0 and SH_0 modes at the notch are visible from the in-plane displacement snapshots (Fig. 3). As the S_0 mode has the faster group velocity, it can be easily distinguished as the outer pulse, having propagated further from the defect at the center of the scattered wave pattern. The horizontal forward and backward pulses for the U_1 component contain the main scattered energy of the S_0 mode with mostly radial displacement, but some amplitude in all directions can be observed for the U_2 component. The SH_0 mode shows four lobes at about 45° orientation to the incident wave direction for both the U_1 and U_2 displacement snapshots, due to the tangential motion relative to the radial propagation direction. The potential for baseline-free measurements can be observed, as the incident A_0 mode does not have any in-plane displacement at the half-thickness of the plate.

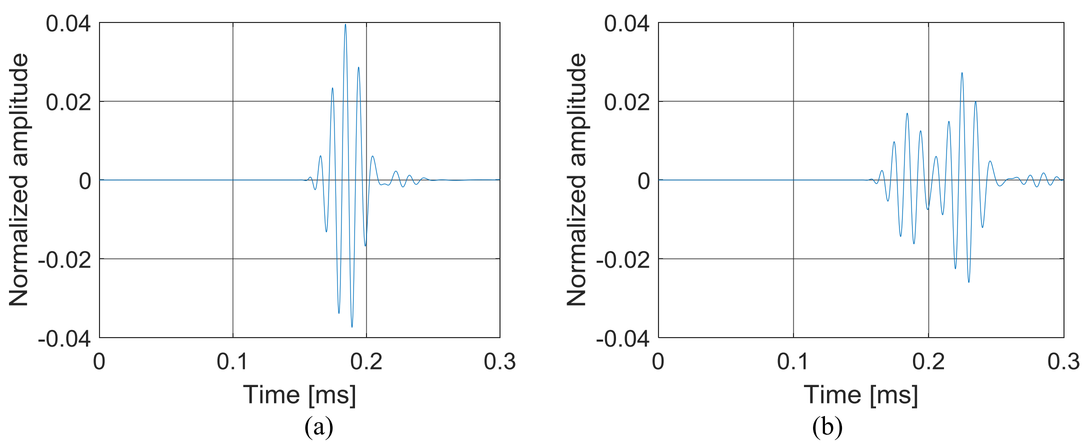

Figure 4. Time traces (normalized), showing U_1 displacement at monitoring points (300mm radius from defect) in (a) 0°; (b) 45° directions.

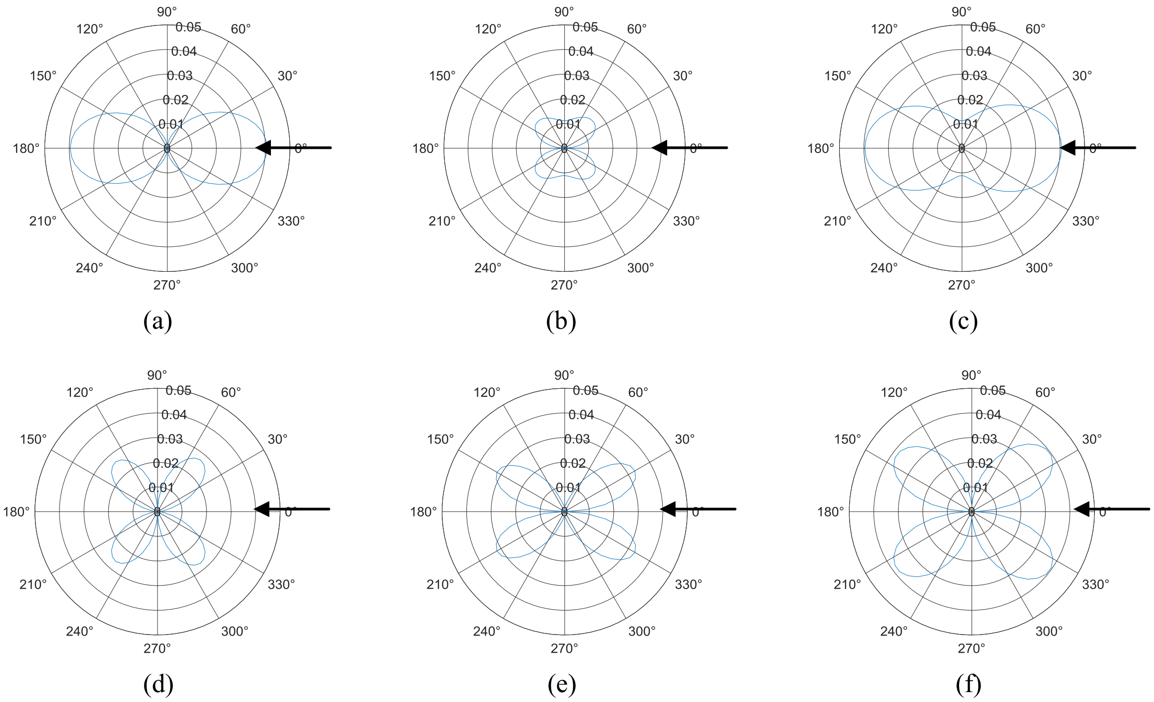

Figure 5. Polar plots of normalized amplitude (300mm monitoring radius) at defect 20mm length, incident wave direction 0° (indicated by arrow), 2.5mm depth; S_0 mode with cut-off time up to 0.21ms: (a) U_1 component; (b) U_2 component; (c) combination; SH_0 mode with cut-off time from 0.21ms: (d) U_1 component; (e) U_2 component; (f) combination.

The amplitude of the scattered, mode converted waves was extracted on a radius of 300mm by interpolating between monitoring nodes on the Cartesian mesh to obtain an amplitude value every 5°. Typical time traces are shown in Fig. 4, with the S_0 mode at 0.16ms dominating in the 0° direction, while in the 45° direction both the faster S_0 and slower SH_0 mode have approximately similar amplitude. Using a cut-off time of 0.21ms was suitable to separate the S_0 and SH_0 modes. Both pulses were separately time windowed and the complex magnitude at the center excitation frequency of 100kHz was extracted using FFT. All amplitudes were normalized relative to out-of-plane amplitude of the A_0 mode incident wave at the defect central location without a defect.

Figure 5 shows the corresponding polar plots of normalized amplitude for the scattered S_0 and SH_0 modes after time separation. Both modes have an U_1 and U_2 displacement component, and the respective amplitudes were combined to give respectively the radial and tangential displacement of the S_0 and SH_0 modes. For the S_0 mode, the forward and backward scattered waves almost have the same amplitude and shape, and the field is symmetric relative to the y-axis (Fig. 5(c)). Two main lobes with about 0.04 (normalized) amplitude are observed along the x-axis (0° and 180° direction). For the SH_0 mode, the amplitude along the x-axis and y-axis is very low (Fig. 5(f)), and the scattering is mostly in the four diagonal directions. The scattered waves with maximum (normalized) amplitude of 0.04 are observed in the diagonal 45°, 135°, 225° and 315° directions.

4. INVESTIGATION OF INFLUENCE OF DEFECT PARAMETERS

The influence of the defect depth and length on the scattering patterns and maximum scattered amplitude of the mode converted S_0 guided wave mode were investigated for a perpendicular incident A_0 wave mode from the 0° (horizontal) direction on a vertical defect with variable length and depth. The polar plots show the pattern of the scattered S_0 mode and the scattering and mode conversion are analyzed. The defect length (20mm) was kept the same for the polar plots shown in Fig. 6 with different defect depths ($1/8^{th}$ depth - 0.625mm, ½ depth - 2.5mm and $7/8^{th}$ depth - 4.375mm).

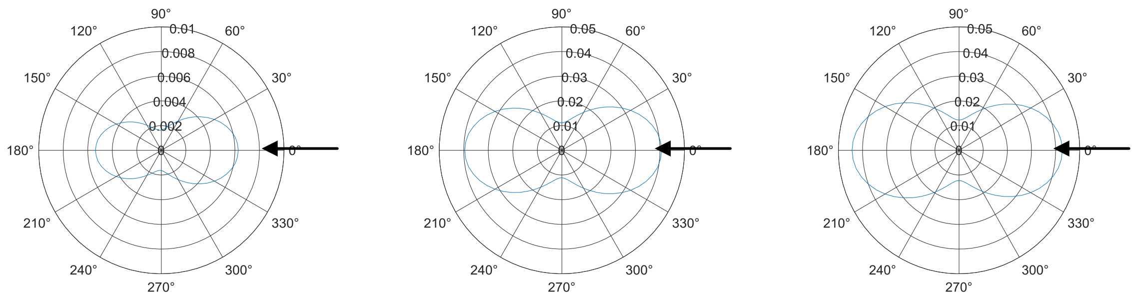

(a) (b) (c)

Figure 6. Polar plots of mode converted S_0 mode amplitude (300mm monitoring radius, normalized) at defect 20mm length, incident wave direction 0° (indicated by arrow); depth: (a) 0.625mm; (b) 2.5mm; (c) 4.375mm.

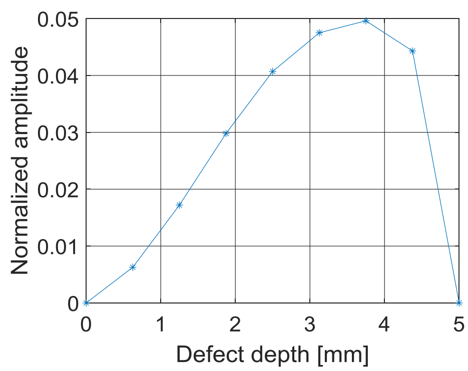

Figure 7. Maximum amplitude of mode converted S_0 mode amplitude (300mm monitoring radius, normalized) at defect 20mm length, incident wave direction 0° for variation of defect depth.

The mode converted S_0 mode scattered amplitude for the perpendicular incident A_0 wave is dominated by two (forward and backward) lobes with slightly different amplitude. For a very shallow defect (1/8th plate thickness), slightly more backward than forward scattered amplitude is obtained (Fig. 6(a)) than for the half-thickness case with similar amplitudes (Fig. 6(b)). For a very deep defect (7/8th plate thickness), slightly larger forward scattered wave and smaller backward scattered wave is obtained (Fig. 6(c)).

In Fig. 7, the maximum scattered S_0 mode amplitude for varying defect depth is plotted. As the defect becomes more severe (deeper), more scattering occurs, but mode conversion must also be considered. For the through thickness defect, no mode conversion occurs, as shown by the zero amplitude. Most mode conversion should theoretically occur at half thickness (2.5mm) defect depth. As a result of the combination of the two effects, the maximum amplitude occurs at approximately ¾ (3.75mm) defect depth.

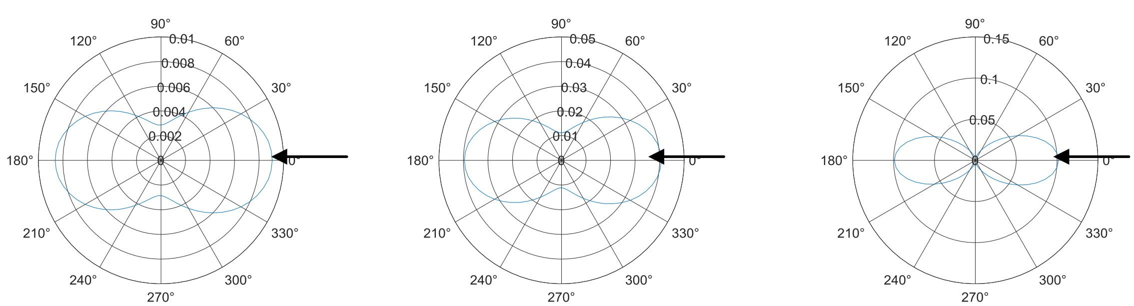

(a) (b) (c)

Figure 8. Polar plots of mode converted S_0 mode amplitude (300mm monitoring radius, normalized) at defect 2.5mm depth, incident wave direction 0° (indicated by arrow); length: (a) 6mm; (b) 20mm; (c) 50mm.

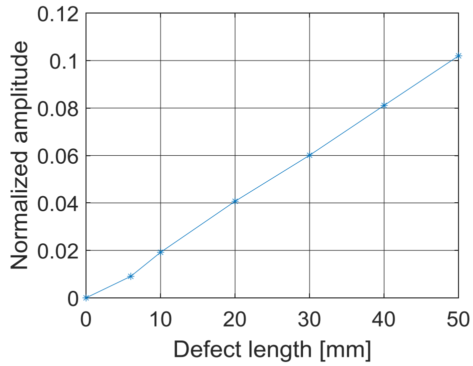

Figure 9. Maximum amplitude of mode converted S_0 mode amplitude (300mm monitoring radius, normalized) at defect 2.5mm depth, incident wave direction 0° for variation of defect length.

The defect depth (2.5mm, half-thickness) and incident wave angle (0°) were kept the same for the polar plots shown in Fig. 8 for different defect lengths (6mm, 20mm and 50mm). The polar plot patterns change as the defect length increases relative to the wavelength, with the two lobes in the 0° to 180° directions increasing in amplitude and becoming more directional (narrow), with less scattered amplitude along the vertical defect orientation. As shown in Fig. 9, the sensitivity (amplitude) of the mode converted S_0 mode increases almost linearly as the defect length increases from 6mm to 50mm. Figure 9 indicates that the normalized amplitude vs length (A_0 to S_0 mode) could potentially be used to predict the defect length for the a given defect depth and incident wave angle (0°), as long as the defect length is shorter than the wavelength of the S_0 mode (54mm).

5. CONCLUSIONS

FE simulations to understand and predict the scattering and mode conversion of an incident, perpendicular A_0 mode to the S_0 and SH_0 modes at part-thickness defects in a plate were conducted and evaluated. For the S_0 mode, two main lobes are observed perpendicular to the defect orientation and the field is symmetric. For the SH_0 mode, the scattering pattern has four lobes in the diagonal directions. Results for the influence of defect size on the detection sensitivity and scattering patterns for the S_0 mode were obtained. Slightly larger forward and smaller backward scattered wave is observed for deep defects and slightly smaller forward and larger backward scattered wave is observed for shallow defects. The maximum amplitude of the mode converted S_0 mode occurs at approximately ¾ plate thickness. The sensitivity of the mode converted S_0 mode continually increases as the defect length increases for the half thickness defect case. Experimental validation will be required and the influence of the incident wave direction on the detection results should be investigated. The mode conversion at the part-thickness defects allows for the potential to develop baseline-free SHM methodology.

REFERENCES

[1] Bhaumik, S.K., Sujata, M. and Venkataswamy, M.A. "Fatigue failure of aircraft components." Engineering Failure Analysis **15**(6):675-694 (2008).

[2] Gurgen, S., Kushan, M.C. and Diltemiz, S.F. "Fatigue failure in aircraft structural components." Handbook of Materials Failure Analysis with Case Studies from the Aerospace and Automotive Industries 261-277 (2016).

[3] Marusic, Z., Bartulovic, D. and Makovic, B. "Methods to detect and prevent fatigue in aging aircraft structures." Tehnicki Vjesnik-Technical Gazette **22**(3):793-803 (2015).

[4] Gholizadeh, S. " A review of non-destructive testing methods of composite materials." Procedia Structural Integrity **1**:50-57 (2016).

[5] Su, Z. Q., Ye, L. and Lu, Y. "Guided Lamb waves for identification of damage in composite structures: A review." Journal of Sound and Vibration **295**(3-5):753-780 (2006).

[6] Rose, J.L. Ultrasonic Guided Waves in Solid Media. Cambridge University Press (2014).

[7] Hayat, K. and Ha, S.K. "Low-velocity impact-induced delamination detection by use of the S-0 guided wave mode in cross-ply composite plates: A numerical study." Journal of Mechanical Science and Technology **28**(2):445-455 (2014).

[8] Fromme, P. Guided Wave Testing. In: Ida, N., Meyendorf, N. (eds) Handbook of Advanced Nondestructive Evaluation. Springer, Cham (2019)
[9] Lowe, M.J.S. and Diligent, O. "Low-frequency reflection characteristics of the s(0) Lamb wave from a rectangular notch in a plate." Journal of the Acoustical Society of America **111**(1):64-74 (2002).
[10] Lowe, M.J.S., Cawley, P., Kao, J.Y. and Diligent, O. "The low frequency reflection characteristics of the fundamental antisymmetric Lamb wave alpha(0) from a rectangular notch in a plate." Journal of the Acoustical Society of America **112**(6):2612-2622 (2002).
[11] Demma, A., Cawley, P. and Lowe, M. "Scattering of the fundamental shear horizontal mode from steps and notches in plates." Journal of the Acoustical Society of America **113**(4):1880-1891 (2003).
[12] Lu, Y., Ye, L., Su, Z.Q. and Yang, C.H. "Quantitative assessment of through-thickness crack size based on Lamb wave scattering in aluminium plates." NDT & E International **41**(1):59-68 (2008).
[13] Fromme, P. "Guided wave sensitivity prediction for part and through-thickness crack-like defects." Structural Health Monitoring **19**(3):953-963 (2020).
[14] Rajagopal, P. and Lowe, M.J.S. "Short range scattering of the fundamental shear horizontal guided wave mode normally incident at a through-thickness crack in an isotropic plate." Journal of the Acoustical Society of America **122**(3):1527-1538 (2007).
[15] Rajagopal, P. and Lowe, M. J. S. "Angular influence on the scattering of fundamental shear horizontal guided waves by a through-thickness crack in an isotropic plate." Journal of the Acoustical Society of America **124**(4):2021-2030 (2008).
[16] Rajagopal, P. and Lowe, M.J.S. "Scattering of the fundamental shear horizontal guided wave by a part-thickness crack in an isotropic plate." Journal of the Acoustical Society of America **124**(5):2895-2904 (2008).
[17] Cho, K. "Estimation of ultrasonic guided wave mode conversion in a plate with thickness variation." IEEE Transactions on Ultrasonics Ferroelectrics and Frequency Control **47**(3):591-603 (2000).
[18] Cegla, F.B., Rohde, A. and Veidt, M. "Analytical prediction and experimental measurement for mode conversion and scattering of plate waves at non-symmetric circular blind holes in isotropic plates." Wave Motion **45**(3):162-177 (2008).
[19] Mori, N., Biwa, S. and Kusak, T. "Damage localization method for plates based on the time reversal of the mode-converted Lamb waves." Ultrasonics **91**:19-29 (2019).
[20] An, Y.K. and Sohn, H. "Experimental Validations of a Baseline-Free Crack Detection Technique using Dual-PZTs." Proceedings of SPIE **7647**:76473R (2010).